

Journal of Biomedical Optics

SPIEDigitalLibrary.org/jbo

Anisotropic light scattering of individual sickle red blood cells

Youngchan Kim
John M. Higgins
Ramachandra R. Dasari
Subra Suresh
YongKeun Park



SPIE

Anisotropic light scattering of individual sickle red blood cells

Youngchan Kim,^a John M. Higgins,^b Ramachandra R. Dasari,^c Subra Suresh,^d and YongKeun Park^a

^aKorea Advanced Institute of Science and Technology, Department of Physics, Daejeon 305-701, Republic of Korea

^bCenter for Systems Biology and Department of Pathology, Massachusetts General Hospital, Boston, Massachusetts 02114, and Department of Systems Biology, Harvard Medical School, Boston, Massachusetts 02115

^cMassachusetts Institute of Technology, George R. Harrison Spectroscopy Laboratory, Cambridge, Massachusetts 02139

^dMassachusetts Institute of Technology, Department of Materials Science and Engineering, Cambridge, Massachusetts 02139

Abstract. We present the anisotropic light scattering of individual red blood cells (RBCs) from a patient with sickle cell disease (SCD). To measure light scattering spectra along two independent axes of elongated-shaped sickle RBCs with arbitrary orientation, we introduce the anisotropic Fourier transform light scattering (aFTLS) technique and measured both the static and dynamic anisotropic light scattering. We observed strong anisotropy in light scattering patterns of elongated-shaped sickle RBCs along its major axes using static aFTLS. Dynamic aFTLS analysis reveals the significantly altered biophysical properties in individual sickle RBCs. These results provide evidence that effective viscosity and elasticity of sickle RBCs are significantly different from those of the healthy RBCs. © 2012 Society of Photo-Optical Instrumentation Engineers (SPIE). [DOI: 10.1117/1.JBO.17.4.040501]

Keywords: red blood cell; sickle cell disease; light scattering; quantitative phase microscopy.

Paper 11736L received Dec. 12, 2011; revised manuscript received Jan. 25, 2012; accepted for publication Feb. 8, 2012; published online Apr. 5, 2012.

Sickle cell disease (SCD) is an inherited blood disorder where a point mutation in the β -globin gene results into production of sickle hemoglobin (HbS) instead of hemoglobin (HbA).¹ Under deoxygenated condition, HbS self-assembles inside the red blood cell (RBC) and dramatically damages the RBC membrane structure, often resulting into a sickle-shaped RBC. This sickle RBC has a considerably reduced deformability, causing abnormal rheological properties of sickle blood and eventually vaso-occlusion and organ damage.

Characterizing sickle cell properties, especially at the single-cell level, plays crucially important roles in understanding the pathophysiology of SCD.² However, the characterization of individual sickle RBCs is complex and not fully addressed. It is presumably because of the limitations of the measurement techniques.² Here, we report both static and dynamic light scattering results from individual sickle RBCs that are enabled

by introducing anisotropic Fourier transform light scattering (aFTLS).

Light scattering techniques have been extensively used for characterizing biological molecules, cells, and tissues.³ Static light scattering can also measure the volume and cytoplasmic hemoglobin concentration of the RBCs.⁴ Temporal fluctuation of scattering signals with respect to a specific scattering angle provides information about motion—a diffusion coefficient of the scattering object.

Angular light scattering has traditionally been measured with goniometer-based instruments and several measurement techniques have been used to study light scattering of objects.^{5,6} Recently, a significant breakthrough in light scattering detection sensitivity has been achieved by the development of Fourier transform light scattering (FTLS) technique.⁷ In FTLS, light scattering patterns from a sample can be obtained from the electric field (E -field) of the sample via quantitative phase imaging technique. The E -field $E(\vec{r}, t)$ is then numerically propagated to far-field by 2-D Fourier transform as $I(\vec{q}, t) = |\iint E(\vec{r}, t) \exp[-j\vec{q} \cdot \vec{r}]|^2 / 2\pi$, where \vec{q} is the spatial frequency vector. The growing scientific interest and increased number of studies using FTLS is indicative of its effectiveness in the study of various phenomena in biophysics and cell biology.^{8–11}

To measure light scattering from sickle RBCs, we prepared blood samples extracted from a patient with SCD as well as from a healthy individual under a research protocol approved by the institutional review board (IRB). The SCD patient was under treatment with hydroxyurea. The blood was collected in ethylenediaminetetraacetic acid (EDTA) anticoagulant and stored at 4°C. For measurement, the blood sample was first diluted with a phosphate-buffered saline. To quantitatively measure the E -field maps of sickle RBCs, we employed diffraction phase microscopy.^{12,13} For each sickle RBC, we measured the E -field $E(\vec{r}, t) = A(\vec{r}, t) \exp[j\Delta\phi(\vec{r}, t)]$, where $A(\vec{r}, t)$ and $\Delta\phi(\vec{r}, t)$ are the amplitude and phase delay, respectively. All the measurements were performed at ambient oxygen concentration (21%) and room temperature (23°C). The time-averaged cell height maps can be retrieved from the measured phase maps as $h(\vec{r}) = \langle \Delta\phi(\vec{r}, t) \rangle \cdot \lambda / (2\pi \cdot \Delta n)$, where λ is the wavelength of the laser and Δn is the difference in refractive index between RBC cytoplasm and surrounding medium. The sickle RBCs are classified in accordance with the morphology: echinocyte (type II), discocyte (type III), and crescent-shaped irreversibly sickled cell (type IV; ISC) (Fig. 1). This classification corresponds with sickle RBC fraction II–IV by density separation.¹⁴ The measured topographies of the sickle cells are consistent with a recent study using quantitative phase imaging.¹⁵

To retrieve anisotropic light scattering, we introduce aFTLS analysis (Fig. 2). We first processed the E -field of individual sickle RBCs such that the horizontal axis of the E -fields is parallel to the long axis of the cell. Then the angular light-intensity scattering pattern of the sickle RBC is retrieved by applying 2D Fourier transformations to the E -field. The spatial frequency vector and the scattering angle can be related as $|\vec{q}| = 2\pi n \sin \theta / \lambda$, where n is the refractive index of medium. The light scattering patterns along the long and short axes are retrieved by selecting the scattering patterns of polar angle width of 30 deg along the horizontal and vertical axes, respectively. Then, the light scattering signals along the long and short axes are retrieved as a function of scattering angle after

Address all correspondence to: YongKeun Park, Korea Advanced Institute of Science and Technology, Department of Physics, Daejeon 305-701, Republic of Korea; E-mail: yk.park@kaist.ac.kr.

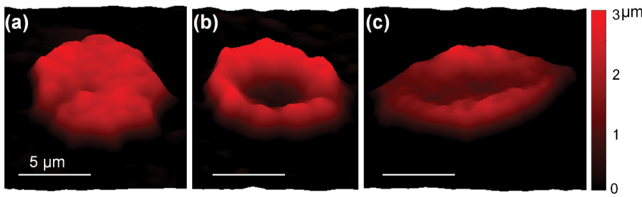


Fig. 1 Topographies of sickle RBCs. (a) echinocyte (type II), (b) discocyte (type III), and (c) crescent-shaped ISC (type IV).

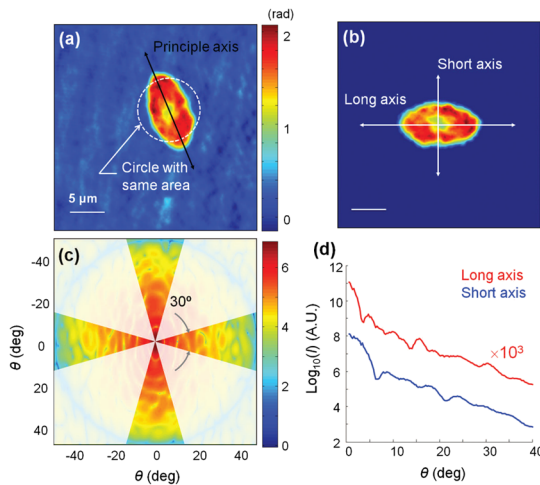


Fig. 2 (a) Phase image of a typical sickle RBC. (b) The long axis is rotated to be aligned with the horizontal axis and the center of mass of the sickle RBC is moved to the center. (c) The retrieved light scattering pattern with the denoted angle ranges for the long and short axes. (d) Light intensity-scattering patterns with respect to the long and short axes of the RBC.

azimuthal average. The ISC showed significantly different scattering signals along the long and short axes [Fig. 2(d)].

We then retrieved the scattering of sickle RBCs in different morphological types (Fig. 3). From the blood extracted from a patient with SCD, we measured 24 cells, 26 cells, and 12 cells of types II, III, and IV, respectively. For comparison purpose, we also measured 25 RBCs from a healthy individual. The sickle RBCs in type IV showed significantly different angular scattering signals the along long and short axes (p -value $< 10^{-5}$) whereas sickle RBCs in types II–III did not show statistically different light scattering signals long those two axes. These anisotropic scattering signals in type IV sickle RBCs can be explained by the crescent- and elongated-shapes.

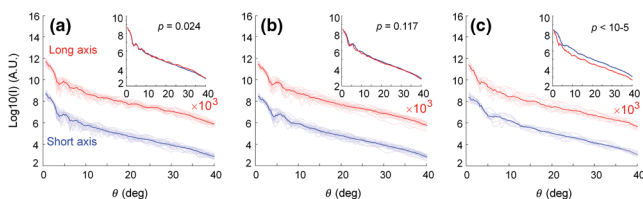


Fig. 3 The static light-intensity scattering patterns associated with individual sickle RBCs of (a) type II, (b) type III, and (c) type IV. Thin lines are from individual sickle RBCs; thick line represents the averaged scattering pattern. The scattering patterns along the long axis are offset up for clarity. (inset) the averaged scattering patterns along short and long axes without offset.

To our knowledge, there has been no prior study of light scattering of individual sickle RBCs in different morphologies. Attempts to measure the angular light scattering from individual sickle RBCs with a goniometer-based instruments or ektacytometers would be extremely challenging because of the following reasons:

1. it is difficult to classify individual sickle RBCs in different morphological groups without imaging the corresponding cell at the microscopic level
2. the scattered power from an individual sickle RBC is very small
3. even if successful in both classification and detection, selection of scattering signal along the long and short axes is difficult without knowing the orientation of the sickle RBC simultaneously.

To measure the dynamic light scattering of sickle RBCs, we measured the E -fields of the sickle RBCs for about 2 s at 120 frames per s. For each E -field, we perform aFTLS analysis, which provide the dynamic light scattering information. We then calculated normalized temporal autocorrelation of the scattering light intensity fluctuations for each scattering angle, $\langle I(\theta, \tau)I(\theta, 0) \rangle / \langle I(\theta, 0) \rangle^2$. Since the spectrum of dynamic light scattering can be described approximately as Lorentzian, its autocorrelation can be expressed as a damped cosine function with a peak frequency ω_0 and a line width Γ as $G(\tau) = A + B \cos(\omega_0 \tau + \varphi) \exp[-\Gamma \tau - \beta^2 \tau^2]$.¹⁶ The phase term φ was added to consider the deviation of the spectrum from an exact Lorentzian function and the β term accounts for instrument deviation.

For sickle RBCs of types II–IV, the intensity autocorrelation was calculated at each scattering angle, from which ω_0 and Γ were retrieved by fitting to the damped cosine function. Then, ω_0 and Γ along the long and short axes are averaged in the range of the specific scattering angle from 0 to 7 deg. The values of ω_0 for all types of sickle RBCs are approximately two times greater than those for the healthy RBCs (p -value $< 10^{-4}$) [Fig. 4(a)]. Between different types in sickle RBCs, ω_0 is not statistically different. The Γ values of sickle RBCs of types II and III are not significantly different from those of the healthy RBCs. However, Γ values of type IV sickle RBCs are significantly smaller than those of the healthy RBCs (p -value < 0.05 ; long axis) [Fig. 4(b)]. The values for ω_0 and Γ did not show statistical difference between the long and short axes; this result implies that the biomechanical properties of the sickle cells do not exhibit anisotropic behavior.

The dynamic light scattering from membrane fluctuations can provide biomechanical properties of the membrane. For a simple flat lipid bilayer, the values for ω_0 and Γ can be directly related to membrane tension and medium viscosity, respectively.¹⁶ However, the human RBC membrane has a complex biconcave shape, and there does not exist a theoretical model relating dynamic light scattering to the mechanical properties of the RBC membrane. Nevertheless, the effective elasticity and effective viscosity of the RBC membrane can be inferred from a peak frequency ω_0 and a line width Γ , respectively.¹⁰ The increase of ω_0 in all types of sickle RBCs indicates the loss of deformability [Fig. 4(a)], which is consistent with previous reports based on measurements using micropipette aspiration and an ektacytometer.^{17,18} This loss of deformability in the sickle RBCs can be explained by alterations in RBC metabolism and membrane structure including loss of membrane

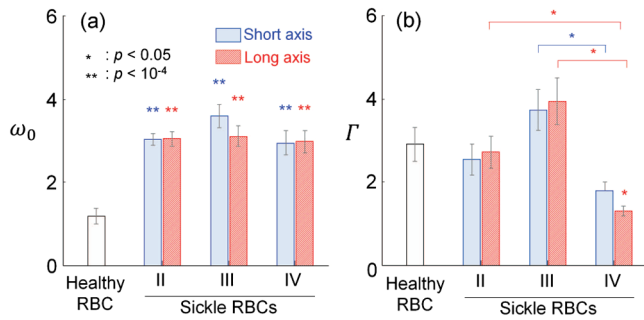


Fig. 4 (a) Peak frequency ω_0 and (b) line width Γ extracted from healthy and sickle RBCs. Error bars indicate the standard errors.

phospholipid symmetry,¹⁹ uncoupling of the lipid bilayer from the sub-membrane structure,²⁰ and abnormal membrane phosphorylation.²¹ Abnormal membrane phosphorylation may seriously affect the enhanced membrane fluctuations in the presence of ATP.^{9,22} The self-assembly of HbS may also decrease the deformability in the sickle RBCs; polymerization of HbS could transform the viscous Hb solution in the sickle RBC cytoplasm into *viscoelastic* material.

Whereas elasticity characterizes resistance to deformation, viscosity characterizes resistance to a rate of deformation. For the RBC, the effective viscosity is associated with the recovery time after large deformation t_c , and it is primarily determined by the shear modulus of the spectrin network μ and the membrane surface viscosity η_m as $t_c = \eta_m/\mu$.²³ The significant decrease in effective viscosity of ISCs, implying a decrease in recovery time, suggests a decrease in η_m or an increase in μ , or both. The increase in η_m may be explained by alterations in the composition or structures of the RBC lipid bilayers or decreased binding of glyceraldehyde phosphate dehydrogenase to the membrane.²⁴ These altered viscoelastic properties of the sickle cell can explain the significantly decreased dynamic fluctuations in the sickle cell membrane.¹⁵

In conclusion, we present anisotropic light scattering of sickle RBCs. The aFTLS technique, a variation of FTLS, precisely and systematically measures anisotropic light scattering of asymmetric small objects. Using aFTLS, we study the light scattering from sickle RBCs and demonstrate anisotropic static light scattering patterns with respect to the elongated shape of sickle RBCs. The dynamic light scattering analysis reveals alterations in mechanical properties depending on the morphological type of sickle RBCs. In the future, the aFTLS technique could be used in combination with other existing optical imaging techniques to better study other RBC related diseases, for example, to understand the protective mechanism of sickle RBCs against infection of malaria parasite.²⁵

Acknowledgments

This work was supported by KAIST (N10110038, N10110048, G04100075), the Korean Ministry of Education, Science and Technology (MEST) Grant No. 2009-0087691 (BRL), National Research Foundation (NRF-2011-355-c00039), and the National Institutes of Health (P41-RR02594-18-24, R01HL094270, and DK083242). YKP acknowledges support from POSCO TJ Park Fellowship.

References

1. M. J. Stuart and R. L. Nagel, "Sickle-cell disease," *Lancet* **364**(9442), 1343–1360 (2004).
2. G. A. Barabino, M. O. Platt, and D. K. Kaul, "Sickle cell biomechanics," *Annu. Rev. Biomed. Eng.* **12**, 345–367 (2010).
3. N. N. Boustany, S. A. Boppart, and V. Backman, "Microscopic imaging and spectroscopy with scattered light," *Annu. Rev. Biomed. Eng.* **12**, 285–314 (2010).
4. N. Mohandas et al., "Accurate and independent measurement of volume and hemoglobin concentration of individual red cells by laser light scattering," *Blood* **68**(2), 506–513 (1986).
5. B. Berne and R. Pecora, *Dynamic Light Scattering: With Applications to Chemistry, Biology, and Physics*, Dover Publications, New York (2000).
6. M. S. Amin et al., "Microrheology of red blood cell membranes using dynamic scattering microscopy," *Opt. Express* **15**(25), 17001–17009 (2007).
7. H. Ding et al., "Fourier transform light scattering of inhomogeneous and dynamic structures," *Phys. Rev. Lett.* **101**(23), 238102 (2008).
8. H. Ding et al., "Optical properties of tissues quantified by Fourier-transform light scattering," *Opt. Lett.* **34**(9), 1372–1374(2009).
9. Y. K. Park et al., "Light scattering of human red blood cells during metabolic remodeling of the membrane," *J. Biomed. Opt.* **16**(1), 011013 (2011).
10. Y. K. Park et al., "Static and dynamic light scattering of healthy and malaria-parasite invaded red blood cells," *J. Biomed. Opt.* **15**(2), 020506 (2010).
11. G. Popescu, *Quantitative Phase Imaging of Cells and Tissues*, McGraw-Hill Professional, New York (2011).
12. Y. K. Park et al., "Diffraction phase and fluorescence microscopy," *Opt. Express* **14**(18), 8263–8268 (2006).
13. G. Popescu et al., "Diffraction phase microscopy for quantifying cell structure and dynamics," *Opt. Lett.* **31**(6), 775–777 (2006).
14. D. K. Kaul et al., "Erythrocytes in sickle cell anemia are heterogeneous in their rheological and hemodynamic characteristics," *J. Clin. Invest.* **72**(1), 22–31 (1983).
15. N. T. Shaked et al., "Quantitative microscopy and nanoscopy of sickle red blood cells performed by wide field digital interferometry," *J. Biomed. Opt.* **16**(3), 030506 (2011).
16. D. Byrne and J. Earnshaw, "Photon correlation spectroscopy of liquid interfaces, I. liquid–air interfaces," *J. Phys. D: Appl. Phys.* **12**(7), 1133–1144 (1979).
17. E. Evans and N. Mohandas, "Membrane-associated sickle hemoglobin: a major determinant of sickle erythrocyte rigidity," *Blood* **70**(5), 1443–1449 (1987).
18. M. P. Sorette, M. G. Lavenant, and M. R. Clark, "Ektacytometric measurement of sickle cell deformability as a continuous function of oxygen tension [published erratum appears in *Blood* 1987 Apr; 69 (4): 1272]," *Blood* **69**(1), 316–323 (1987).
19. F. Kuypers et al., "Detection of altered membrane phospholipid asymmetry in subpopulations of human red blood cells using fluorescently labeled annexin V," *Blood* **87**(3), 1179–1187 (1996).
20. S. C. Liu et al., "Uncoupling of the spectrin-based skeleton from the lipid bilayer in sickled red cells," *Science* **252**(5005), 574–576 (1991).
21. J. K. Dzandu and R. Johnson, "Membrane protein phosphorylation in intact normal and sickle cell erythrocytes," *J. Biol. Chem.* **255**(13), 6382–6386 (1980).
22. Y. K. Park et al., "Metabolic remodeling of the human red blood cell membrane," *Proc. Natl. Acad. Sci.* **107**(4), 1289–1294 (2010).
23. E. Evans and R. Hochmuth, "Membrane viscoelasticity," *Biophys. J.* **16**(1), 1–11 (1976).
24. C. Vasseur et al., "Decreased G3PDH binding to erythrocyte membranes in sickle cell disease," *Nouv. Rev. Fr. Hematol.* **34**(2), 155–161 (1992).
25. S. Cho, S. Kim, Y. Kim, and Y. K. Park, "Optical imaging techniques for the study of malaria," *Trends Biotechnol.* **30**(2), 71–79 (2012).